

1 **Impact of grids and dynamical cores in CESM2.2 on**
2 **the meteorology and climate of the Arctic**

3 **Adam R. Herrington** ¹, **Marcus Lofverstrom** ², **Peter H. Lauritzen** ¹ and
4 **Andrew Gettelman** ¹

5 ¹National Center for Atmospheric Research, 1850 Table Mesa Drive, Boulder, Colorado, USA
6 ²Department of Geosciences, University of Arizona, 1040 E. 4th Street, Tucson, AZ USA

7 **Key Points:**

- 8 • enter point 1 here
9 • enter point 2 here
10 • enter point 3 here

Abstract

[enter your Abstract here]

Plain Language Summary

[enter your Plain Language Summary here or delete this section]

1 Introduction

General Circulation Models (GCMs) are powerful tools for understanding the meteorology and climate of the high-latitudes, which are among the most sensitive regions on Earth to global and environmental change. Despite their importance, the numerical treatment of polar regions in GCMs is handled in vastly-different ways due to the so-called *pole-problem* (D. Williamson, 2007), which refers to numerical instability arising from the convergence of meridians at the polar points on latitude-longitude grids (e.g., Figure 1a). Depending on the numerics, methods exist to suppress this instability, and latitude-longitude grids may be advantageous for polar processes as structures can be represented with more degrees of freedom than elsewhere in the computational domain. With the recent trend towards globally uniform unstructured grids, any potential benefits of latitude-longitude grids on polar regions may become a relic of the past. In this study, a spectrum of model grids and dynamical cores (hereafter referred to as *dycores*) available in the Community Earth System Model, version 2.2 (CESM; <http://www.cesm.ucar.edu/models/cesm2/>) are evaluated to understand their impacts on the simulated characteristics of the Arctic, with a special focus on the meteorology over the Greenland Ice Sheet.

In the 1970's the pole problem was largely defeated through wide-spread adoption of efficient spectral transform methods in GCMs. These methods transform grid point fields into a global, isotropic representation in wave space, where linear operators (e.g. horizontal derivatives) in the equation set can be solved for exactly. While spectral transform methods are still used in the 21st century, local numerical methods have become desirable for their ability to run efficiently on massively parallel systems. The pole-problem has thus re-emerged in contemporary climate models that use latitude-longitude grids, and some combination of reduced grids and polar filters are necessary to ameliorate this instability (Jablonowski & Williamson, 2011). Polar filters are akin to a band-aid; they subdue the growth of unstable modes by applying additional damping to the solution over polar regions. One might expect that this additional damping reduces the effective resolution such that the resolved scales are similar across the entire domain, but this seems unlikely (describe why) and is explored further in this study.

An alternative approach is to use unstructured grids, which allow for more flexible grid structures that permit quasi-uniform grid spacing globally and eliminates the pole-problem entirely (e.g., Figure 1c). This grid flexibility also allows for variable-resolution or regional grid refinement (e.g., Figure 2). Grids can be developed with refinement over polar regions that could in principle make up for any loss in polar resolution in transitioning away from latitude-longitude grids (e.g., Figure 2), although this comes at the cost of a smaller CFL-limiting time-step in the refined region (the CFL-condition — short for Courant–Friedrichs–Lowy condition — is a necessary condition for numerical stability when using discrete data in time and space). However, unstructured grids scale more efficiently on parallel systems than latitude-longitude grids, likely resulting in a greater prevalence of unstructured grids as computing power continued to increase over time.

The meteorology and climate of the Arctic is characterized by a range of processes and scales that are difficult to represent in GCMs (Bromwich et al., 2001; Smirnova & Golubkin, 2017; van Kampenhout et al., 2018). For example, while synoptic scale storms

are generally well represented at typical GCM resolutions of 1 to 2 degrees (Jablonowski & Williamson, 2006; Stocker, 2014), mesoscale Polar Lows are not well resolved at these resolutions. These mesoscale systems are prevalent during the cold season and produce gale-force winds that can induce large heat and moisture fluxes through the underlying sea-ice/ocean interface. The Arctic also contains the Greenland Ice Sheet (hereafter denoted as *GrIS*). While it blankets the largest island in the world (Greenland), many of the processes that control the *GrIS* annual surface mass balance (the integrated sum of precipitation and melting) are only partially resolved at typical GCM resolutions. For example, *GrIS* precipitation is typically confined to the ice-sheet margins (predominately the southeastern margin) where orographic precipitation is generated by steep topographic slopes. Moreover, *GrIS* ablation areas (marginal regions where seasonal melting exceeds the annual mass input from precipitation) are typically 10s to 100 km wide and confined to low-level areas or regions with limited precipitation. GCMs struggle to resolve the magnitude and extent of these features (van Kampenhout et al., 2018), which can lead to unrealistic ice sheet growth in models with an interactive ice sheet component (e.g., Lofverstrom et al., 2020).

The goal of this study is to characterize the representation of high-latitude regions using the spectral-element and finite-volume dycores in CESM2.2, as these models treat the high-latitudes, e.g., the pole-problem, in different ways. The manuscript is laid out as follows: Section 2 consists of documentation of the grids, dycores and physical parameterizations used in this study. The Arctic refined grids were developed by the authors, and this section serves as their official documentation in CESM2.2. Section 2 also contains a description of the experiments along with reanalysis datasets and post-processing software used for evaluating the model simulations. Section 3 contains the results of the experiments, followed by Section 4 that provides a general discussion and conclusions.

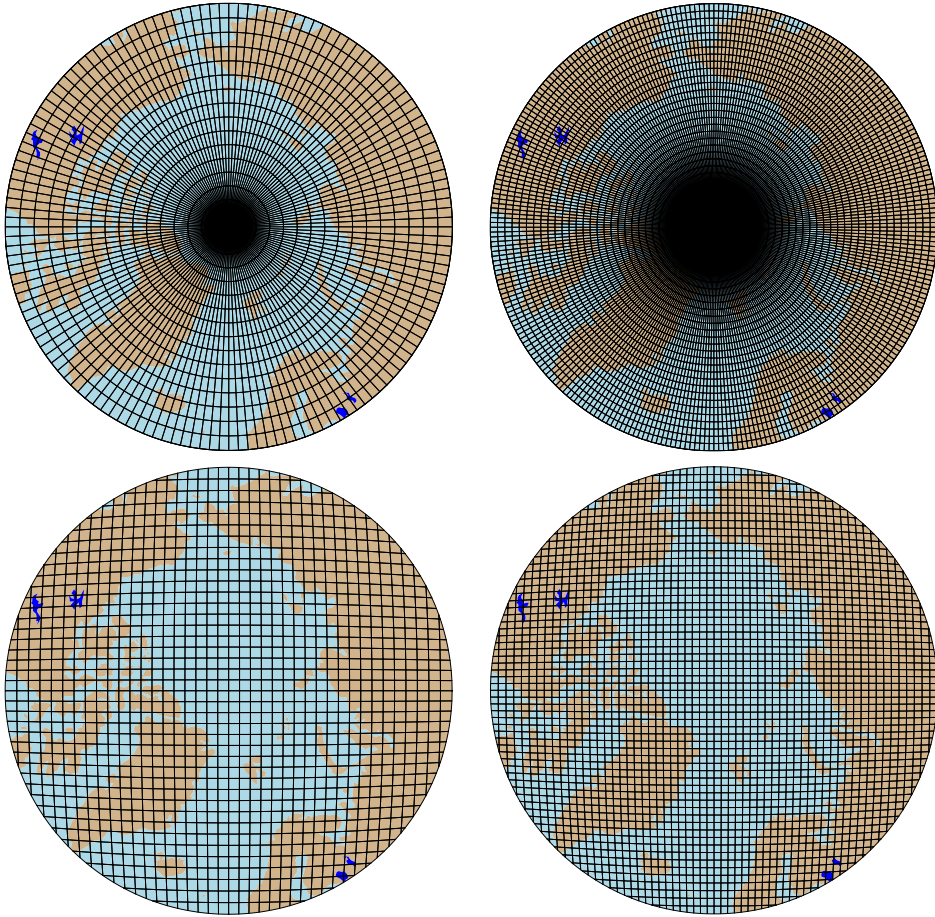
2 Methods

2.1 Dynamical cores

The atmospheric component of CESM2.2, the Community Atmosphere Model, version 6.3 (CAM; <https://ncar.github.io/CAM/doc/build/html/index.html>), supports a number of different atmospheric dynamical cores. These include dycores using latitude-longitude grids, such as finite-volume (FV; Lin, 2004) and eulerian spectral transform (EUL; Collins et al., 2006) models, and dycores built on unstructured grids, including spectral-element (SE; Lauritzen et al., 2018) and finite-volume 3 (FV3; Putman & Lin, 2007) models. The EUL dycore is the oldest dycore in CAM, and the least supported of all the dycores in the current model. FV3 is the newest dycore in CAM, but it was not fully incorporated at the time this work commenced; both the EUL and FV3 dycores are omitted from this study. As such, the results presented in this study are comparing the performance of the SE and FV dycores.

2.1.1 Finite-volume (FV) dynamical core

The FV dycore is a hydrostatic model that integrates the equations of motion using a finite-volume discretization on a spherical latitude-longitude grid (Lin & Rood, 1997). The 2D dynamics evolve in floating Lagrangian layers that are periodically mapped to Eulerian reference grid in the vertical (Lin, 2004), using a hybrid-pressure vertical coordinate. Hyperviscous damping is applied to the divergent modes while Laplacian damping is applied to momentum in the top few layers, referred to as a *sponge layer* (Lauritzen et al., 2011). A polar filter is used to avoid computational instability due to the convergence of the meridians, allowing for a more practical time-step. It takes the form of a Fourier filter in the zonal direction, with the damping coefficients increasing monotonically in the poleward direction (Suarez & Takacs, 1995).

**Figure 1.** .

108 ***2.1.2 Spectral-element (SE) dynamical core***

109 The SE dycore is a hydrostatic model that integrates the equations of motion us-
 110 ing a high-order continuous Galerkin method (Taylor et al., 1997; Dennis et al., 2012).
 111 The computational domain is a cubed-sphere grid tiled with quadrilateral elements (e.g.,
 112 Figure 2). Each element contains a fourth order basis set in each horizontal direction,
 113 with the solution defined at the roots of the basis functions, the Gauss-Lobatto-Legendre
 114 (GLL) quadrature points. This results in 16 GLL nodal points within each element, with
 115 12 of the points lying on the (shared) element boundary. Communication between el-
 116 ements happens via the direct stiffness summation (Canuto et al., 2007), which applies
 117 a numerical flux to the element boundaries that reconciles overlapping nodal values and
 118 produces a continuous global basis set.

119 As with the FV dycore, the dynamics evolve in floating Lagrangian layers that are
 120 subsequently mapped to an Eulerian reference grid. A dry mass vertical coordinate was
 121 more recently implemented for thermodynamic consistency with condensates (Lauritzen
 122 et al., 2018). The 2D dynamics have no implicit dissipation and so hyperviscosity op-
 123 erators are applied to all prognostic variables to remove spurious numerical errors (Dennis
 124 et al., 2012). Laplacian damping is applied in the sponge layer.

125 The SE dycore supports regional grid refinement via its variable-resolution config-
 126 uration, requiring two enhancements over uniform resolution grids. (1) As the numer-

**Figure 2.**

ical viscosity increases with resolution, explicit hyperviscosity relaxes according to the local element size, reducing in strength by about an order of magnitude per halving of the grid spacing. A tensor-hyperviscosity formulation is used (Guba et al., 2014), which adjusts the coefficients in two orthogonal directions to more accurately target highly distorted quadrilateral elements. (2) The topography boundary conditions need to be smoothed in a way that does not excite grid scale modes, and so the NCAR topography software (Lauritzen et al., 2015) was modified to scale the smoothing radius by the local element size.

For spectral-element grids with quasi-uniform grid spacing, a variant in which tracer advection is computed using the Conservative Semi-Lagrangian Multi-tracer transport scheme (CSLAM) is used instead (Lauritzen et al., 2017). CSLAM has improved tracer property preservation and accelerated multi-tracer transport. It uses a separate grid from the spectral-element dynamics, through dividing each element into 3×3 control volumes with quasi-equal area. The physical parameterizations are computed from the state on the CSLAM grid, which has clear advantages over the default SE dycore in which the physics are evaluated at the GLL nodal points (A. Herrington et al., 2018).

2.2 Grids

Six grid are evaluated in this study (Table X). The FV dycore is run with 1° and 2° grid spacing, referred to as *f09* and *f19*, respectively (Figure 1a,b). The 1° equivalent of the CAM-SE-CSLAM grid is also run, referred to as *ne30pg3* (Figure 1c), where *ne* refers to a grid with of $ne \times ne$ elements per cubed-sphere face, and *pg* denotes that there are $pg \times pg$ control volumes per element for computing the physics. An additional 1° CAM-SE-CSLAM grid is run, but with the physical parameterizations computed on a grid that contains 2×2 control volumes per element, *ne30pg2* (Figure 1d; A. R. Herrington et al., 2019).

Two variable resolution meshes were developed as part of the CESM2.2 release that contains grid refinement over the Arctic (Figure 2). The Arctic meshes were developed using the software package SQuadgen (<https://github.com/ClimateGlobalChange/squadgen>). The *ARCTIC* grid is a 1° grid with $\frac{1}{4}^\circ$ regional refinement over the broader Arctic region. The *ARCTICGRIS* grid is identical to the *ARCTIC* grid, but contains an additional patch covering the big island of Greenland with $\frac{1}{8}^\circ$ resolution.

158 2.3 Physical parameterizations

159 The CAM6 physical parameterization package (hereafter referred to as the *physics*;
 160 <https://ncar.github.io/CAM/doc/build/html/index.html>) is used for all simula-
 161 tions in this study. CAM6 physics is most noteably different from it's predecessors through
 162 the incorporation of high-order turbulence closure, Cloud Layers Unified by Binormals
 163 (CLUBB; Golaz et al., 2002; Bogenschutz et al., 2013), which jointly acts as a PBL, shal-
 164 low convection and cloud macrophysics scheme. CLUBB is coupled with the MG2 mi-
 165 crophysics scheme (Gettelman et al., 2015), with prognostic precipitation and classical
 166 nucleation theory in representing cloud ice for improved cloud-aerosol interactions. Deep
 167 convection is parameterized using a convective quasi-equilibrium mass flux scheme (Zhang
 168 & McFarlane, 1995; Neale et al., 2008) inclusing convective momentum transport (Richter
 169 et al., 2010). PBL form drag is modeled after (Beljaars et al., 2004) and orographic grav-
 170 ity wave drag is represented with an anisotropic method informed by the orientation of
 171 topographic ridges at the sub-grid scale.

172 The CAM convention is that the physics package determines the vertical resolu-
 173 tion. Since all runs use CAM6 physics, all grids and dycores use 32 levels in the verti-
 174 cal, with a model top of about 1 hPa or about 40 km. The physics time-step, in con-
 175 trast, is dependent on grid resolution. Increases in horizontal resolution permit faster
 176 vertical velocities that reduce characteristic time-scales, and so the physics time-step should
 177 be reduced to avoid large time truncation errors (A. Herrington & Reed, 2018). The *ARCTIC*
 178 and *ARCTICGRIS* grids are therefore run with a 4× and 8× reduction in physics time-
 179 step relative to the default 1800 s time-step used in coarser, uniform resolution grids.

180 2.4 Experimental design

181 All grids and dycores are run using an identical transient 1979-1998 AMIP-style
 182 configuration, with prescribed monthly SST/sea-ice after (Hurrell et al., 2008). This con-
 183 figuration refers to the *FHIST compset* and runs out of the box in CESM2.2. The Com-
 184 munity Land Model (CLM5; [https://escomp.github.io/ctsm-docs/versions/release](https://escomp.github.io/ctsm-docs/versions/release-clm5.0/html/users_guide/index.html)
 185 -clm5.0/html/users_guide/index.html), which uses the same grid as the atmosphere
 186 grid, calculates the surface energy balance at each land tile within a grid cell, which is
 187 used to compute snow and bare ice melting to inform the surface mass balance (SMB)
 188 of a glacier unit (van Kampenhout et al., 2020). Ice accumulation is modeled as a cap-
 189 ping flux, or snow in excess of the assumed 10 m snow cap, and refreezing of liquid within
 190 the snowpack additionally acts as a source of mass in the SMB calculation. Since the
 191 10 m snowcap needs to be reached in the accumulation zone to simulate the SMB, the
 192 snow depths in the variable-resolution grids were spun-up by forcing CLM5 offline, cy-
 193 cling over 20 years of a fully coupled *ARCTIC* run for about 500 years. The uniform
 194 resolution grids are all initialized with an SMB from an existing *f09* spun-up initial con-
 195 dition.

196 3 Results

197 3.1 Tropospheric temperatures

198 Before delving into the simulated characteristics of the Arctic, an understanding
 199 of the global mean differences between the grids and dycores are assessed, Figure 3 shows
 200 the climatological, zonal mean height plots expressed as differences between the uniform
 201 resolution grids and dycores. The *f09* grid is warmer than the *f19* grid, primarily in the
 202 mid-to-high latitudes and throughout the depth of the troposphere. This is a common
 203 response to increasing horizontal resolution in GCMs (Pope & Stratton, 2002; Roeck-
 204 ner et al., 2006), and (A. R. Herrington & Reed, 2020) has shown that this occurs in CAM
 205 due to greater resolved vertical velocities that in turn, facilitate greater condensational
 206 heating in the macrophyiscs routine in CLUBB. The right columns in Figure 3 supports

207 this interpretation, which shows an increase in the climatological CLUBB heating in the
208 mid-latitudes in the *f*09 grid.

209 As the SE dycore is less diffusive than the FV dycore, the resolved vertical velocities
210 are larger in the SE dycore, and so a modest, resolution-like sensitivity occurs in
211 which *ne30pg3* is warmer than *f*09 (Figure 3). The stratosphere has a different response,
212 in which *ne30pg3* is much cooler than *f*09 in the mid-to-high latitudes. The differences
213 in temperature between *ne30pg3* and *ne30pg2* are small, with a slight warming near the
214 tropopause at high latitudes. This is consistent with the similar climates found between
215 these grids in (A. R. Herrington et al., 2019).

216 Comparing the variable-resolution grids to the uniform resolution grids is compli-
217 cated because we are simultaneously increase the grid resolution and reducing the physics
218 time-step, both which noticeably impact the solution (D. L. Williamson, 2008). An ad-
219 dditional *ne30pg3* simulations is run with the physics time-step used in the *ARCTIC* grid,
220 referred to as *ne30pg3**. Figure 4 shows the change in climatological temperature in zonal-
221 mean height space between *ne30pg3** and *ne30pg3*. A similar warming response to in-
222 creasing resolution occurs when the time-step is reduced, and the mechanism is similar
223 in that the shorter time-step facilitates greater condensational heating by CLUBB. Fig-
224 ure 4 shows the difference in climatological temperature between the *ARCTIC* grid and
225 the *ne30pg3** grid. The greater condensational heating and warmer temperatures are con-
226 fined to the regionally refined region when the impact of physics time-steps is removed
227 from the analysis.

228 **3.2 Inter-annual variability**

229 **3.3 Synoptic-scale storm characteristics**

230 **3.4 Orographic gravity waves emanating from Greenland**

231 **3.5 Katabatic winds emanating from Greenland**

232 **3.6 Greenland surface mass balance**

233 **4 Conclusions**

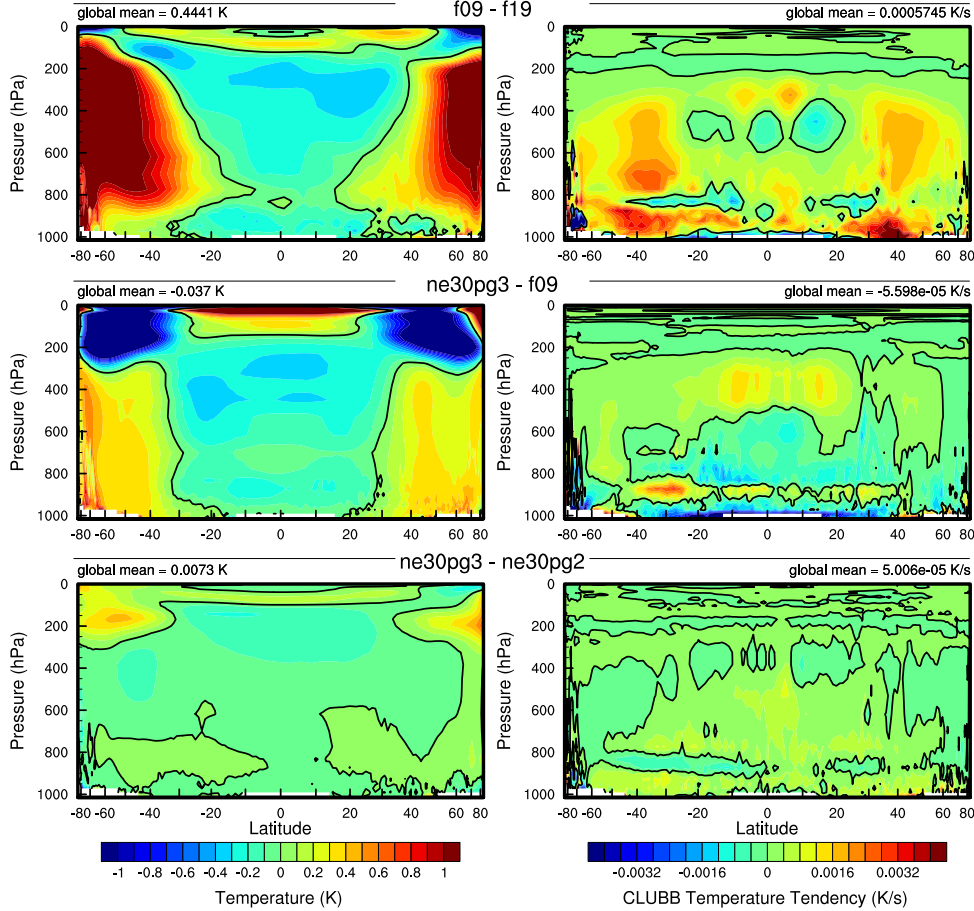
234 **Acknowledgments**

235 This material is based upon work supported by the National Center for Atmospheric Re-
236 search (NCAR), which is a major facility sponsored by the NSF under Cooperative Agree-
237 ment 1852977. Computing and data storage resources, including the Cheyenne super-
238 computer (doi:10.5065/D6RX99HX), were provided by the Computational and Infor-
239 mation Systems Laboratory (CISL) at NCAR.

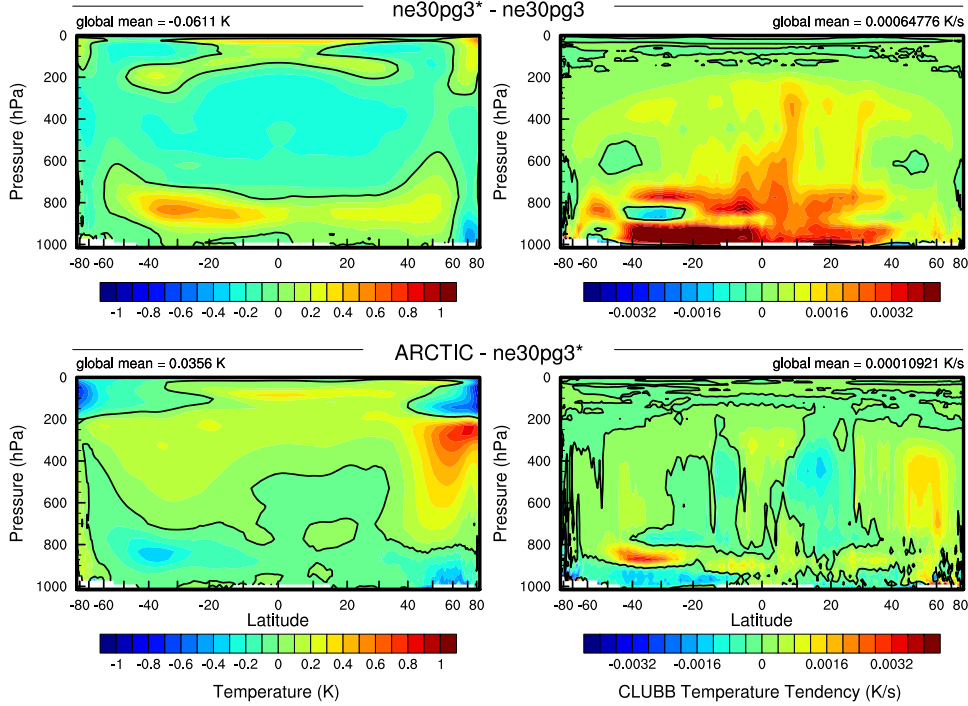
240 The data presented in this manuscript is available at <https://github.com/adamrher/>
241 2020-arcticgrids.

242 **References**

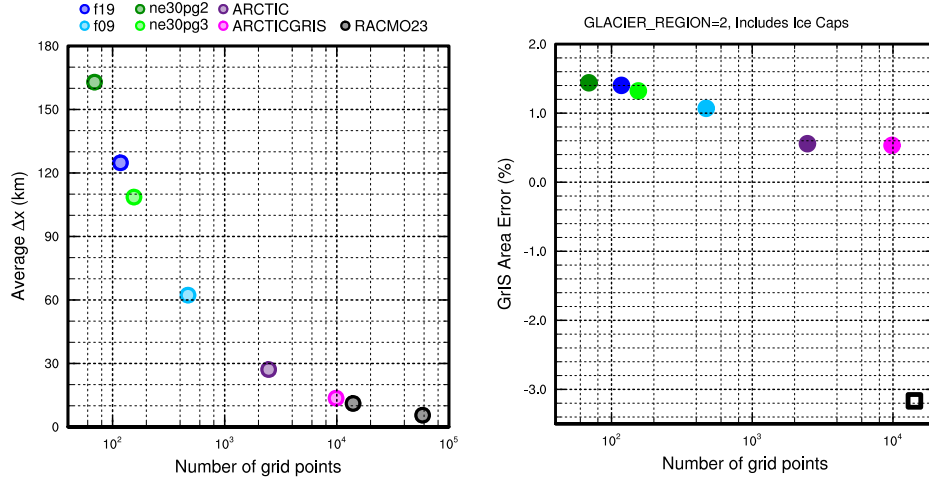
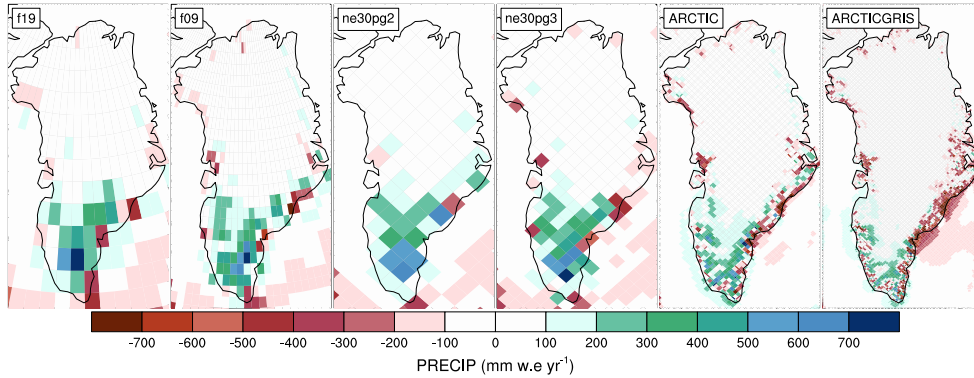
- 243 Beljaars, A., Brown, A., & Wood, N. (2004). A new parametrization of turbulent
244 orographic form drag. *Quart. J. Roy. Meteor. Soc.*, 130(599), 1327–1347. doi:
245 10.1256/qj.03.73
- 246 Bogenschutz, P. A., Gettelman, A., Morrison, H., Larson, V. E., Craig, C., & Scha-
247 nen, D. P. (2013). Higher-order turbulence closure and its impact on climate
248 simulations in the community atmosphere model. *Journal of Climate*, 26(23),
249 9655–9676.
- 250 Bromwich, D. H., Cassano, J. J., Klein, T., Heinemann, G., Hines, K. M., Steffen,
251 K., & Box, J. E. (2001). Mesoscale modeling of katabatic winds over greenland

**Figure 3.**

- with the polar mm5. *Monthly Weather Review*, 129(9), 2290–2309.
- Canuto, C., Hussaini, M. Y., Quarteroni, A., & Zang, T. (2007). *Spectral methods: Evolution to complex geometries and applications to fluid dynamics* (1st ed.). Springer.
- Collins, W. D., Rasch, P. J., Boville, B. A., Hack, J. J., McCaa, J. R., Williamson, D. L., ... Zhang, M. (2006). The formulation and atmospheric simulation of the community atmosphere model version 3 (cam3). *Journal of Climate*, 19(11), 2144–2161.
- Dennis, J. M., Edwards, J., Evans, K. J., Guba, O., Lauritzen, P. H., Mirin, A. A., ... Worley, P. H. (2012). CAM-SE: A scalable spectral element dynamical core for the Community Atmosphere Model. *Int. J. High. Perform. C.*, 26(1), 74–89. Retrieved from <http://hpc.sagepub.com/content/26/1/74.abstract> doi: 10.1177/1094342011428142
- Gettelman, A., Morrison, H., Santos, S., Bogenschutz, P., & Caldwell, P. (2015). Advanced two-moment bulk microphysics for global models. part ii: Global model solutions and aerosol–cloud interactions. *Journal of Climate*, 28(3), 1288–1307.
- Golaz, J.-C., Larson, V. E., & Cotton, W. R. (2002). A pdf-based model for boundary layer clouds. part i: Method and model description. *Journal of the Atmospheric Sciences*, 59(24), 3540–3551. doi: 10.1175/1520-0469(2002)059<3540:apbmfb>2.0.co;2

**Figure 4.**

- 273 Guba, O., Taylor, M. A., Ullrich, P. A., Overfelt, J. R., & Levy, M. N. (2014). The
 274 spectral element method (sem) on variable-resolution grids: evaluating grid
 275 sensitivity and resolution-aware numerical viscosity. *Geosci. Model Dev.*, 7(6),
 276 2803–2816. doi: 10.5194/gmd-7-2803-2014
- 277 Herrington, A., Lauritzen, P., Taylor, M. A., Goldhaber, S., Eaton, B. E., Bacmeis-
 278 ter, J., ... Ullrich, P. (2018). Physics-dynamics coupling with element-based
 279 high-order galerkin methods: quasi equal-area physics grid. *Mon. Wea. Rev.*,
 280 47, 69–84. doi: 10.1175/MWR-D-18-0136.1
- 281 Herrington, A., & Reed, K. (2018). An idealized test of the response of the commu-
 282 nity atmosphere model to near-grid-scale forcing across hydrostatic resolutions.
 283 *J. Adv. Model. Earth Syst.*, 10(2), 560–575.
- 284 Herrington, A. R., Lauritzen, P. H., Reed, K. A., Goldhaber, S., & Eaton, B. E.
 285 (2019). Exploring a lower resolution physics grid in cam-se-cslam. *Journal of*
 286 *Advances in Modeling Earth Systems*, 11.
- 287 Herrington, A. R., & Reed, K. A. (2020). On resolution sensitivity in the commu-
 288 nity atmosphere model. *Quarterly Journal of the Royal Meteorological Society*,
 289 146(733), 3789–3807.
- 290 Hurrell, J. W., Hack, J. J., Shea, D., Caron, J. M., & Rosinski, J. (2008). A new
 291 sea surface temperature and sea ice boundary dataset for the community at-
 292 mosphere model. *Journal of Climate*, 21(19), 5145–5153.
- 293 Jablonowski, C., & Williamson, D. L. (2006). A baroclinic instability test case for
 294 atmospheric model dynamical cores. *Q. J. R. Meteorol. Soc.*, 132, 2943–2975.
- 295 Jablonowski, C., & Williamson, D. L. (2011). The pros and cons of diffusion, fil-
 296 ters and fixers in atmospheric general circulation models., in: P.H. Lauritzen,
 297 R.D. Nair, C. Jablonowski, M. Taylor (Eds.), Numerical techniques for global
 298 atmospheric models. *Lecture Notes in Computational Science and Engineering*,
 299 Springer, 80.

**Figure 5.****Figure 6.** Climatological (1979–1998) annual precipitation rate bias relative to the RACMO2.3p2 5.5km resolution data product (Noël et al., 2019).

- 300 Lauritzen, P. H., Bacmeister, J. T., Callaghan, P. F., & Taylor, M. A. (2015). Ncar
301 global model topography generation software for unstructured grids. *Geosci-
302 entific Model Development Discussions*, 8(6), 4623–4651. doi: 10.5194/gmdd-8
303 –4623–2015
- 304 Lauritzen, P. H., Mirin, A., Truesdale, J., Raeder, K., Anderson, J., Bacmeister, J.,
305 & Neale, R. B. (2011). Implementation of new diffusion/filtering operators
306 in the CAM-FV dynamical core. *Int. J. High Perform. Comput. Appl.*. doi:
307 10.1177/1094342011410088
- 308 Lauritzen, P. H., Nair, R., Herrington, A., Callaghan, P., Goldhaber, S., Dennis, J.,
309 ... Dubos, T. (2018). NCAR CESM2.0 release of CAM-SE: A reformulation
310 of the spectral-element dynamical core in dry-mass vertical coordinates with
311 comprehensive treatment of condensates and energy. *J. Adv. Model. Earth
312 Syst.*. doi: 10.1029/2017MS001257
- 313 Lauritzen, P. H., Taylor, M. A., Overfelt, J., Ullrich, P. A., Nair, R. D., Goldhaber,
314 S., & Kelly, R. (2017). CAM-SE-CSLAM: Consistent coupling of a conser-
315 vative semi-lagrangian finite-volume method with spectral element dynamics.
316 *Mon. Wea. Rev.*, 145(3), 833–855. doi: 10.1175/MWR-D-16-0258.1
- 317 Lin, S.-J. (2004). A 'vertically Lagrangian' finite-volume dynamical core for global

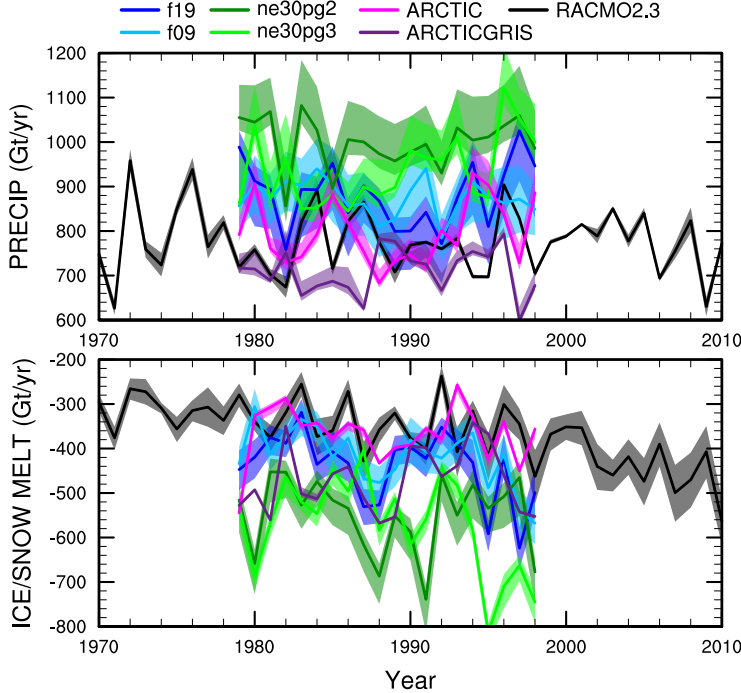
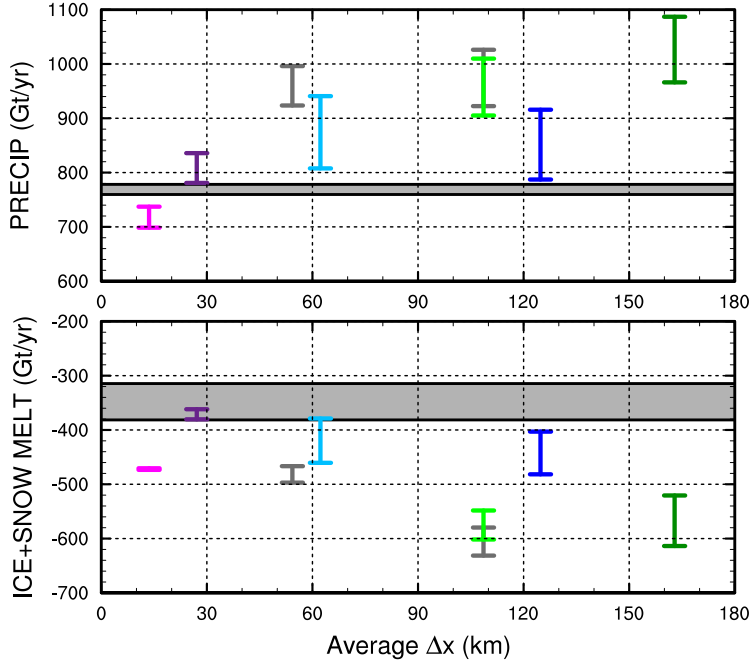


Figure 7. Time-series of annual (solid+liquid) precipitation (top) and annual runoff (bottom) integrated over the Greenland Ice Sheet for all six simulations and compared to RACMO3.2. The raw fields are mapped to two target low resolution grids, f19 & ne30pg2, and using two different remapping methods, conservative ESMF and high order TempestRemap. The remapped values are then integrated over the ice mask of the target grid. This gives four time-series for each simulation (three for f19 & ne30pg2), with the mean value given by the solid line and shading spanning the extent of the remapped solutions.

- 318 models. *Mon. Wea. Rev.*, 132, 2293-2307.
- 319 Lin, S.-J., & Rood, R. B. (1997). An explicit flux-form semi-Lagrangian shallow-
320 water model on the sphere. *Q.J.R.Meteorol.Soc.*, 123, 2477-2498.
- 321 Lofverstrom, M., Fyke, J. G., Thayer-Calder, K., Muntjewerf, L., Vizcaino, M.,
322 Sacks, W. J., ... Bradley, S. L. (2020). An efficient ice sheet/earth sys-
323 tem model spin-up procedure for cesm2-cism2: Description, evaluation, and
324 broader applicability. *Journal of Advances in Modeling Earth Systems*, 12(8),
325 e2019MS001984.
- 326 Neale, R. B., Richter, J. H., & Jochum, M. (2008). The impact of convection on
327 ENSO: From a delayed oscillator to a series of events. *J. Climate*, 21, 5904-
328 5924.
- 329 Noël, B., van de Berg, W. J., Lhermitte, S., & van den Broeke, M. R. (2019). Rapid
330 ablation zone expansion amplifies north greenland mass loss. *Science advances*,
331 5(9), eaaw0123.
- 332 Pope, V., & Stratton, R. (2002). The processes governing horizontal resolution sensi-
333 tivity in a climate model. *Climate Dynamics*, 19(3-4), 211-236.
- 334 Putman, W. M., & Lin, S.-J. (2007). Finite-volume transport on various cubed-
335 sphere grids. *J. Comput. Phys.*, 227(1), 55-78.
- 336 Richter, J. H., Sassi, F., & Garcia, R. R. (2010). Toward a physically based gravity
337 wave source parameterization in a general circulation model. *J. Atmos. Sci.*,

**Figure 8.** .

- 67, 136-156. doi: dx.doi.org/10.1175/2009JAS3112.1
- 338 Roeckner, E., Brokopf, R., Esch, M., Giorgetta, M., Hagemann, S., Kornblueh, L.,
 339 ... Schulzweida, U. (2006). Sensitivity of simulated climate to horizontal
 340 and vertical resolution in the echam5 atmosphere model. *Journal of Climate*,
 341 19(16), 3771–3791.
- 342 Smirnova, J., & Golubkin, P. (2017). Comparing polar lows in atmospheric reanalyses: Arctic system reanalysis versus era-interim. *Monthly Weather Review*,
 343 145(6), 2375–2383.
- 344 Stocker, T. (2014). *Climate change 2013: the physical science basis: Working group i contribution to the fifth assessment report of the intergovernmental panel on climate change*. Cambridge university press.
- 345 Suarez, M. J., & Takacs, L. L. (1995). Volume 5 documentation of the aries/geos dynamical core: Version 2.
- 346 Taylor, M. A., Tribbia, J., & Iskandarani, M. (1997). The spectral element method
 347 for the shallow water equations on the sphere. *J. Comput. Phys.*, 130, 92-108.
- 348 van Kampenhout, L., Lenaerts, J. T., Lipscomb, W. H., Lhermitte, S., Noël, B.,
 349 Vizcaíno, M., ... van den Broeke, M. R. (2020). Present-day greenland ice sheet
 350 climate and surface mass balance in cesm2. *Journal of Geophysical Research: Earth Surface*, 125(2), e2019JF005318.
- 351 van Kampenhout, L., Rhoades, A. M., Herrington, A. R., Zarzycki, C. M., Lenaerts,
 352 J. T. M., Sacks, W. J., & van den Broeke, M. R. (2018). Regional grid refinement
 353 in an earth system model: Impacts on the simulated greenland surface
 354 mass balance. *The Cryosphere Discuss.* doi: 10.5194/tc-2018-257
- 355 Williamson, D. (2007). The evolution of dynamical cores for global atmospheric
 356 models. *J. Meteor. Soc. Japan*, 85, 241-269.
- 357 Williamson, D. L. (2008). Convergence of aqua-planet simulations with increasing
 358 resolution in the community atmospheric model, version 3. *Tellus A*, 60(5),
 359 848–862. doi: 10.1111/j.1600-0870.2008.00339.x
- 360 Zhang, G., & McFarlane, N. (1995). Sensitivity of climate simulations to the pa-

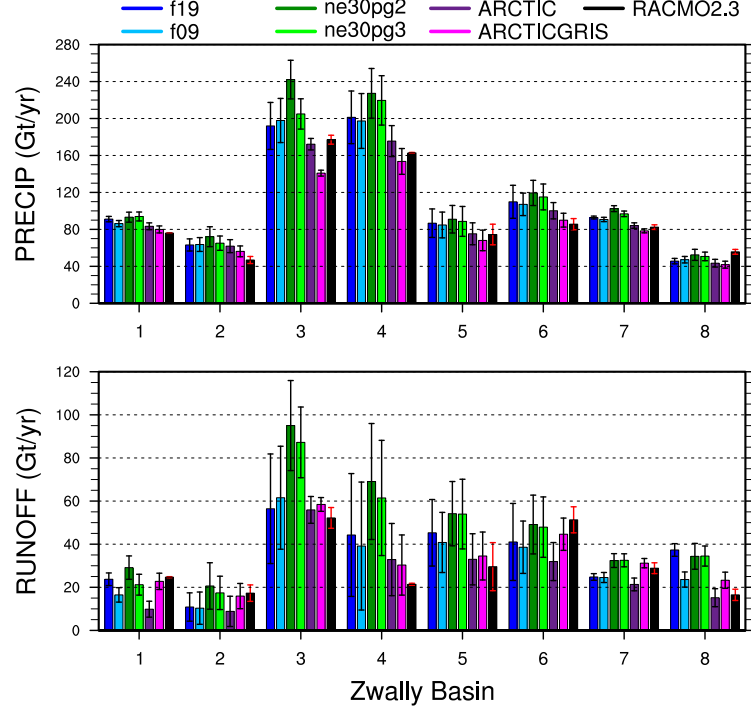


Figure 9.

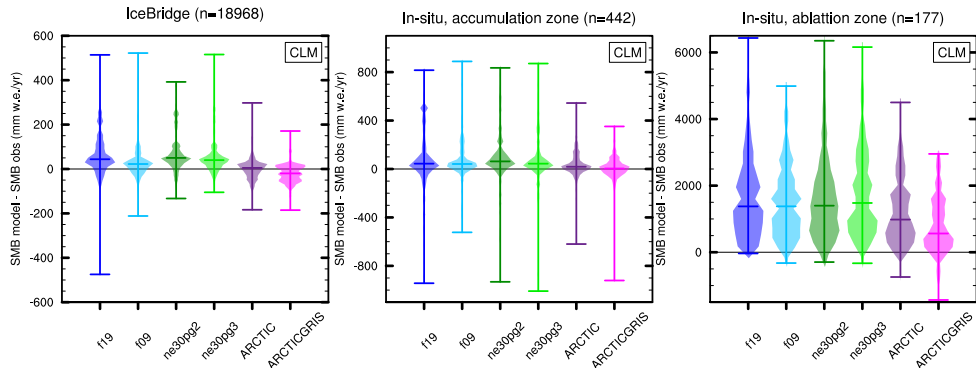


Figure 10.

367
368 ramentization of cumulus convection in the canadian climate centre general
circulation model. *Atmosphere-ocean*, 33(3), 407-446.

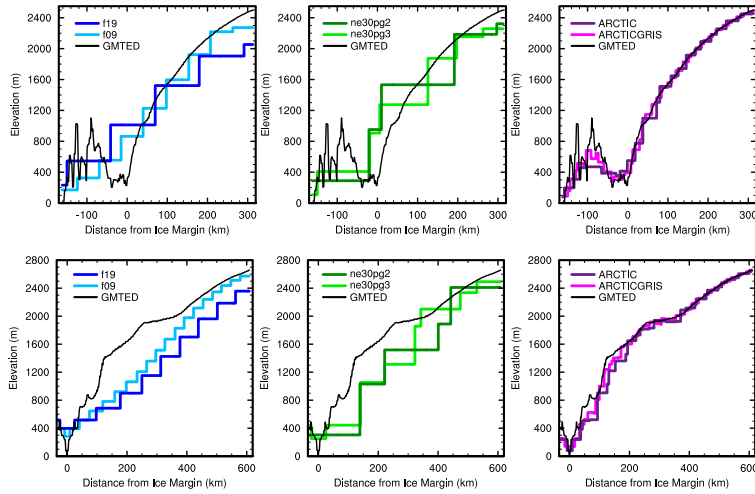


Figure 11. .

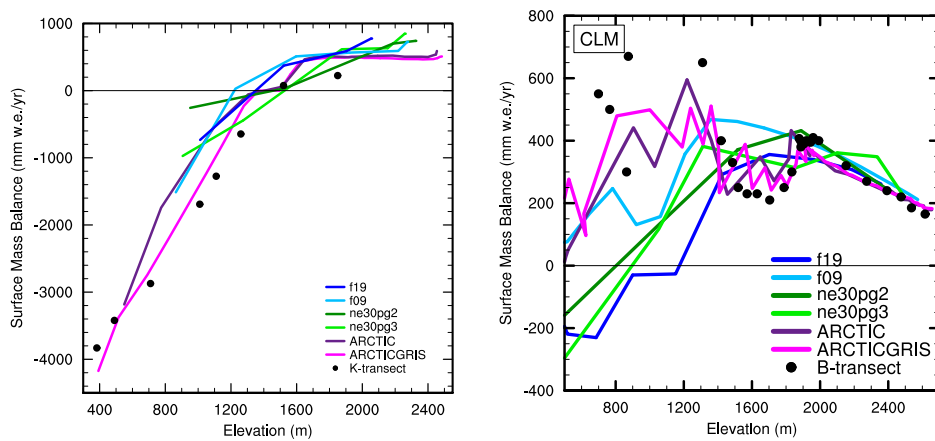


Figure 12. .